

On-Device Self-Supervised Learning of Low-Latency Monocular Depth from Only Events

Jesse J. Hagenaars¹Yilun Wu¹Federico Paredes-Vallés²Stein Stroobants¹Guido C.H.E. de Croon¹¹ MAVLab, TU Delft² Sony Europe Ltd.

Abstract

Event cameras provide low-latency perception for only milliwatts of power. This makes them highly suitable for resource-restricted, agile robots such as small flying drones. Self-supervised learning based on contrast maximization holds great potential for event-based robot vision, as it foregoes the need to high-frequency ground truth and allows for online learning in the robot’s operational environment. However, online, onboard learning raises the major challenge of achieving sufficient computational efficiency for real-time learning, while maintaining competitive visual perception performance. In this work, we improve the time and memory efficiency of the contrast maximization learning pipeline. Benchmarking experiments show that the proposed pipeline achieves competitive results with the state of the art on the task of depth estimation from events. Furthermore, we demonstrate the usability of the learned depth for obstacle avoidance through real-world flight experiments. Finally, we compare the performance of different combinations of pre-training and fine-tuning of the depth estimation networks, showing that on-board domain adaptation is feasible given a few minutes of flight.

1. Introduction

Event cameras capture per-pixel changes in brightness at microsecond resolution, while consuming only milliwatts of power [13]. This enables low-latency perception and decision making in environments even when undergoing large visual motion, on platforms that are constrained in power budget, such as small drones.

To make full use of the temporal information in the event stream, the learning pipeline consisting of network architecture and loss function should also operate at high frequency [24]. Ground truth for variables like optical flow or depth is often only available at lower rates of 10–20 Hz [5, 14, 37]. While some datasets allow upsampling

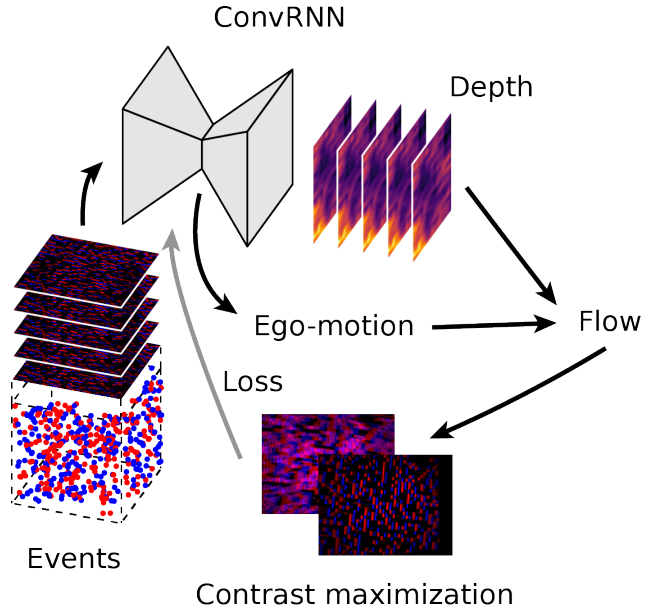


Figure 1. Self-supervised learning pipeline to estimate dense depth from event-camera data. We improve the time and memory efficiency of the pipeline for enabling online learning onboard of a small drone. This leads to better depth estimates and more successful obstacle avoidance behavior.

of ground truth to higher rates [3, 37], reaching the temporal resolution of an event camera might be difficult and come at the cost of high data rates. This holds back supervised learning at the short time scales perceivable with event cameras.

Contrast maximization [11] allows self-supervised learning of optical flow, depth and ego-motion from events alone [12, 24, 27, 38]. Because no ground truth is needed, learning and prediction can be done at frequencies of 100 Hz [24] or even 200 Hz [25], with the only limit being the network’s ability to integrate temporal information long enough to capture sufficient motion for learning.

A major advantage of self-supervised learning is that it foregoes the time- and pain-staking process of obtaining ground truth. This enables learning to scale up to enormous datasets. An additional, but typically less emphasized advantage is that self-supervised learning can in principle be performed in the operational environment of a robot or other edge device. Such online, self-supervised learning greatly reduces the need for generalization of the learned model, as training happens directly on data sampled from the test distribution [29]. For visual tasks such as monocular depth estimation, this is particularly important, as generalization of this perceptual capability to different environments than the training environment is notoriously difficult [10, 31]. Online, self-supervised learning does bring additional challenges. The first, main challenge is that not only the network but also the learning framework should be computationally efficient enough to run onboard.

In this work, we improve the efficiency of the pipeline such that on-device learning of low-latency monocular depth and ego-motion becomes feasible. We demonstrate continual learning on-board a small flying drone, and show the usability of the resulting depth for obstacle avoidance. Furthermore, we investigate various combinations of pre-training and on-board learning. When trained on event camera datasets, our small recurrent network shows state-of-the-art depth estimation performance among self-supervised approaches. Our work scratches at the unused potential of on-board, online self-supervised learning, promising smaller reality gaps, leading to better performance.

2. Related work

2.1. (Self-/Un)supervised monocular depth estimation

Self-supervised and unsupervised learning of monocular depth has garnered significant attention since the early works that focused on joint depth-pose estimation for static scenes [16, 30, 36]. These foundational studies have spurred further advancements to handle more complex scenarios, such as dynamic scenes, by integrating optical flow estimation [26, 35], leveraging regularization techniques [21], or incorporating motion segmentation [28]. Additionally, several studies have explored learning camera parameters [6, 17], which is particularly relevant for on-device learning scenarios with unknown cameras.

Wang *et al.* [33] demonstrate that recurrent networks can enhance depth estimation by effectively utilizing information from multiple frames, resulting in more consistent depth scale predictions. Similarly, Bian *et al.* [2] introduce a loss term to encourage scale consistency, addressing a critical challenge in depth estimation. Achieving depth predictions with a consistent scale significantly enhances the

stability of robot control systems relying on these depth estimates. By combining recurrent architectures and scale-consistent training, our approach aligns with these advancements, offering a robust solution for dynamic, on-device learning during real-world operation.

2.2. Contrast maximization to learn from events

The contrast maximization framework enables the extraction of accurate optical flow information by leveraging the temporal misalignment of accumulated events [11, 12]. This optical flow can be estimated either through model-based methods [27] or using neural networks [18, 24, 38]. The choice of the optical flow model itself offers a spectrum of possibilities, ranging from linear models [18, 38], to segmented representations [24], and even parametrized trajectories [19].

In our work, we adopt the approach outlined in [24], as it aligns with our goal of achieving high-frequency estimation using a neural network. This method is particularly well-suited for handling event trajectories that may exhibit nonlinear patterns, which are common in dynamic and complex scenarios. By using a neural network trained to extract optical flow from event data, we aim to ensure both flexibility and accuracy in environments where traditional linear assumptions might fail.

Moreover, this approach supports efficient inference, which is critical for real-time applications such as robotic navigation or on-device learning. The ability to accommodate nonlinear event trajectories further broadens its applicability, making it a robust choice for extracting motion information from event-based sensors in challenging conditions.

2.3. Self-supervised event-based depth estimation

Early works focused on jointly estimating depth and pose directly from events, employing either contrast maximization techniques [38] or photometric error methods based on event frames [34]. A notable contribution by Zhu *et al.* was their ability to estimate metric depth through the incorporation of a stereo loss term, enabling absolute depth recovery. These methods demonstrated the potential of event-based sensing for depth and pose estimation in static scenes.

More recent research has expanded these approaches to address dynamic scenes [15], where traditional static-scene assumptions do not hold, and developed more principled frameworks for model-based contrast maximization to jointly estimate depth, ego-motion, and optical flow [27]. These advancements represent a significant step toward understanding and processing complex, real-world motion using event data.

Additionally, some works have explored the integration of intensity images as either inputs or components of the loss function [39]. This hybrid approach leverages the com-

plementary information provided by intensity images to enhance the performance of event-based depth estimation, especially in scenarios where pure event data might lack sufficient structure or texture information.

2.4. On-device (learning of) depth estimation

Already in 2016, Lamers *et al.* [20] demonstrated the feasibility of learning depth estimation onboard a small flapping-wing drone. Although their approach did not produce dense depth maps, it proved effective for navigation, marking an early milestone in on-device learning for aerial robotics.

More recent advancements have focused on generating dense depth maps onboard drones. Liu *et al.* [22] developed a system to estimate depth from images for obstacle avoidance on a tiny quadrotor, leveraging recorded real-world datasets for training. Bhattacharya *et al.* [1], on the other hand, used a simulation-based approach to train depth estimation from events. They successfully transitioned to real-world applications by performing offline fine-tuning on real-world data, enabling effective obstacle avoidance in practice.

In this work, we take a distinct approach by performing fine-tuning onboard the drone in an online fashion during flight, adapting the model in real time while actively avoiding obstacles. This method combines the strengths of self-supervised learning with real-time adaptability, paving the way for more robust and efficient systems capable of handling dynamic environments. By eliminating the reliance on extensive offline fine-tuning or pre-collected datasets, our approach addresses the challenges of real-world deployment more directly.

3. Method

3.1. Optical flow from contrast maximization

Contrast maximization [11, 12] assumes events $\mathcal{E} = \{e_k\}$ are triggered by motion, meaning that a warp $e_k = (t_k, \mathbf{x}_k, p_k) \mapsto e'_k = (t_{\text{ref}}, \mathbf{x}'_k, p_k)$ with the correct motion estimate will align it with other events triggered by the same portion of a moving edge, increasing the contrast of the image of warped events (IWE).

We follow the contrast maximization framework as in [24], which estimates optical flow for thin slices of the event stream using a recurrent architecture. By concatenating flows \mathbf{u}_i as $\Delta \mathbf{x}_k = \sum_i (\Delta t_i \mathbf{u}_i)(e_k)$, events can be warped iteratively to neighbouring slices, with the correct flows leading to sharp IWEs at all reference times along the trajectory:

$$\mathcal{L}_{\text{CM}} = \frac{1}{T+1} \sum_{t_{\text{ref}}=0}^T \frac{\sum_k \bar{t}_k(t_{\text{ref}}) \kappa(\mathbf{x}_k)}{\sum_k \kappa(\mathbf{x}_k)} \quad (1)$$

where $\bar{t}_k(t_{\text{ref}})$ is the timestamp contribution of event e_k to the IWE at reference time t_{ref} , and κ is a bilinear splatting

kernel. We regularize (prevent event collapse) by scaling IWEs by the number of pixels with at least one event and by masking events that get warped out of the image space at any point [18, 24].

3.2. Combining depth and ego-motion into flow

Assuming a static scene and no occlusion/disocclusion, depth and ego-motion can be accurately estimated from monocular video alone [36]. The optical flow used to warp a pixel \mathbf{x} between different views is constructed from depth D and a camera transformation or relative pose P :

$$\mathbf{x}' \sim KPD(\mathbf{x})K^{-1}\mathbf{x} \quad (2)$$

with K the camera intrinsic matrix, P consisting of a rotation R and a translation \mathbf{t} , and \sim because depth is only defined up to a scale.¹ The network estimates depth D directly using a softplus activation [17]; relative pose P is estimated with rotation expressed in exponential coordinates ω [32], and converted to R using Rodrigues' formula.

To encourage consistent scale for consecutive depth predictions, we include the geometry consistency loss from [2], which computes a normalized difference between the forward-projected depth $D_{0 \rightarrow 1}$ and interpolated depth D'_1 for all valid pixels $\mathbf{x} \in V$ (visible in both images):

$$\mathcal{L}_{\text{geo}} = \frac{1}{|V|} \sum_{\mathbf{x} \in V} \frac{|D_{0 \rightarrow 1}(\mathbf{x}) - D'_1(\mathbf{x})|}{D_{0 \rightarrow 1}(\mathbf{x}) + D'_1(\mathbf{x})} \quad (3)$$

where we average over the number of valid pixels $|V|$. Setting an appropriate weight λ , this then results in the full loss formulation as:

$$\mathcal{L} = \mathcal{L}_{\text{CM}} + \lambda \mathcal{L}_{\text{geo}} \quad (4)$$

3.3. Optimizations for on-device learning

For efficient prediction, we make use of a relatively small, 430k-parameter network. It consists of a strided convolutional encoder, a ConvGRU recurrent bottleneck, and a two-tailed convolutional decoder for depth and ego-motion (more details in the supplementary material). While one network forward pass takes less than a millisecond on an NVIDIA RTX 4090, computing the contrast maximization loss and backpropagating the resulting gradients each take up more than 10 ms.

To make on-device learning feasible, we have to improve the efficiency of the components that make up the loss computation and network update: i) warping all events in the accumulated set of events \mathcal{E} using a sampled optical flow to all reference times $t_{\text{ref}} \in [0, T]$, ii) splatting them to the IWE at that t_{ref} , iii) computing the gradient with respect to the network parameters.

¹For simplicity, we omit the conversion to homogeneous coordinates.

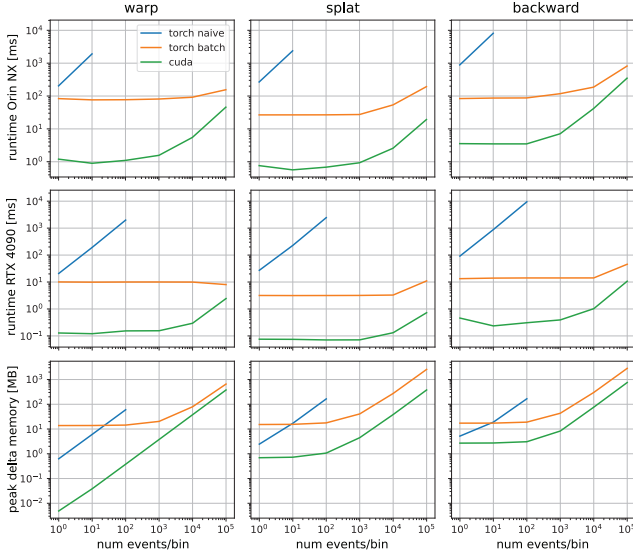


Figure 2. Runtime and peak increase in memory consumption for different phases of computing the contrast maximization loss on an NVIDIA RTX 4090 and Jetson Orin NX (log-scale). Naive PyTorch processes all events in a for-loop. While batching events together improves a lot over this, parallel processing of all events in CUDA results in even bigger speedups with less memory consumed.

Previous work [24] warped and splatted events in batches using PyTorch functions. This has multiple inefficiencies. Batching different amounts of events together leads to padding with zeros, resulting in wasteful computation and memory usage. This also goes for warping events that already went out of the image space (and therefore do not contribute to the loss anymore). Furthermore, PyTorch does not have an optimized implementation for bilinear splatting, meaning you have to implement it yourself. This results in extra computations and memory consumption for things like automatic differentiation.

The abovementioned issues can be resolved by considering that all events independently contribute to the loss because they are summed in the IWEs, and that we can therefore parallelize over all the accumulated events \mathcal{E} . We implement the functions to do so in CUDA, and connect them to PyTorch as an extension. As is shown in Fig. 2, the resulting improvements are, depending on the device, roughly 100x in terms of runtime. Common datasets like UZH-FPV [9] and MVSEC [37] have between 1k and 10k events per bin, well within the range of these speedups. Furthermore, looking at the peak delta memory, we can see that not needing padding allows much lower memory consumption when event data is highly sparse. Because we now provide the analytical gradients in the CUDA backward kernel, these do not have to be computed through automatic differentiation, leading to efficiency improvements for the back-

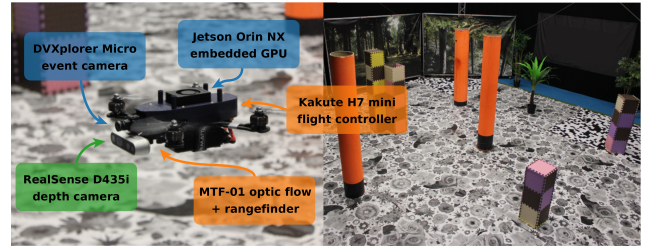


Figure 3. Overview of the drone (left) and the flight environment (right). System components in blue are for the on-board depth learning pipeline, orange components are for low-level flight control, and green components are for logging only.

ward pass.

3.4. Using depth for obstacle avoidance

In the absence of metric depth and with a possibly varying scale, we can construct simple obstacle-avoiding behaviour using the difference in predicted depths for different parts of the field-of-view [4, 22]. More specifically, we slice the depth map into K vertical bins, compute the average inverse depth d_k for each, and use these to set a desired yaw rate $\dot{\psi}$:

$$\dot{\psi} = \dot{\psi}_{\text{goal}}(\mathbf{d}) + \dot{\psi}_{\text{avoid}}(\mathbf{d}) \quad (5)$$

$$\dot{\psi}_{\text{goal}}(\mathbf{d}) = \lambda_{\text{goal}} \left(\arg \min_k (d_k) - \bar{k} \right) \quad (6)$$

$$\dot{\psi}_{\text{avoid}}(\mathbf{d}) = \lambda_{\text{avoid}} \sum_{k=0}^{K-1} (\bar{k} - k) e^{-\frac{\alpha}{d_k}} e^{-\frac{(k-\bar{k})^2}{2\sigma^2}} \quad (7)$$

where yawing to the right is positive, and $\bar{k} = \frac{K-1}{2}$ is the center index. The resulting behaviour is both obstacle-avoiding (avoid part) and depth-seeking (goal part).

3.5. Robot

The experimental setup as shown in Fig. 3 consists of a custom 5-inch quadrotor with a total weight of approximately 800 g, including all sensors, actuators, on-board compute, and battery. All algorithms are implemented to run entirely onboard, leveraging an NVIDIA Jetson Orin NX embedded GPU to obtain data from the event-camera, perform learning and estimate depth in real-time. Control commands (yaw rate) based on the predicted depth maps are sent to the flight controller, a Kakute H7 mini running the open-source autopilot software PX4.² Communication between PX4 and the Orin is done using ROS2 [23]. An MTF-01 optic flow sensor and rangefinder enable stable autonomous flight where only yaw rate is controlled by the depth pipeline.

To keep the event rate down (around 1 Mev/s), we only turn on every fourth pixel on the DVXplorer Micro, resulting in a 160x120 stream (instead of 640x480) for the same

²<https://px4.io/>

Depth Cutoff	outdoor_day1			outdoor_night1		
	10m	20m	30m	10m	20m	30m
Zhu et al. [39] ³	1.40	2.07	2.65	2.18	2.70	3.64
Zhu et al. [39]	3.90	<u>3.79</u>	4.89	5.55	4.57	5.72
Zhu et al. [38]	<u>2.72</u>	3.84	<u>4.40</u>	3.13	<u>4.02</u>	4.89
Ours	2.25	3.36	4.23	<u>3.25</u>	3.83	4.50
Ours (Dense)	1.96	2.67	3.29	2.92	3.56	4.28

Table 1. MAE (mean absolute error) of depth prediction in meters on MVSEC test sequences at various depth cutoff distances. The best result is highlighted in bold, and the second best is underlined. The method shown in the shaded row serves as a reference and is not directly comparable to the others, as it also uses image frames.

		1PE	2PE	MAE	RMSE
SL	Cho et al. [8]	8.966	2.345	0.501	1.175
	DSEC Baseline [14]	10.92	2.905	0.576	1.381
SSL	Ours (best scale)	82.64	66.57	4.583	5.937
	Ours (approx. scale)	84.92	70.47	4.946	6.274

Table 2. Quantitative evaluation on DSEC disparity benchmark. Due to the lack of other SSL (self-supervised learning) methods on the leaderboard, we compare against two representative SL (supervised learning) methods.

field-of-view. These events are accumulated into 20 ms windows and made into a frame for the network. The whole events-to-depth pipeline is running at approximately 30 Hz while learning, consuming on average around 15 W. We include a RealSense D435i depth camera for logging purposes only. To plot ground-truth flight trajectories, we record the drone’s position using a motion capture system.

4. Experiments

4.1. Benchmarks

We train our proposed network on the training sets (detailed training sequences provided in the supplementary materials) with a batch size of 8 and a constant learning rate of 1e-4 with the Adam optimizer for 50 epochs. The quantitative evaluations on MVSEC and DSEC are provided in Tab. 1 and Tab. 2.

On MVSEC, our method outperforms the other two self-supervised, events-only baselines [38, 39]. For context, we also provide the results from the approach in [39], which additionally uses intensity frames in the training process for a photometric consistency loss. Although it achieves a higher accuracy, our networks rely solely on event streams during training. For completeness, we also assess the accuracy of dense depth (i.e., not masked by events), as shown in the

³The network uses events as input but was trained with intensity frames in the loss function. Therefore, it is included as a reference but is not directly comparable to self-supervised methods trained solely on event data.

last row of Tab. 1.

In the absence of self-supervised methods on the DSEC disparity benchmark, we compare our approach against two top-performing stereo-event-based supervised learning baselines [7, 14]. To convert our monocular unnormalized depth predictions from our network output into metric depth, we apply a scaling factor derived from the ratio of the median predicted depth to the ground truth median from the training set, labeled as “approx. scale” in Tab. 2. Additionally, we conduct a grid search on the scaling factor to achieve the highest accuracy on the test set, reported as “best scale”.

While our accuracy on the DSEC disparity benchmark falls short of supervised baselines, qualitative comparisons in Fig. 4 demonstrate that our approach effectively captures meaningful structures within disparity maps, even without ground truth labels during training. Notably, close objects—such as the car in `interlaken_00_a(540)` and traffic signs in `thun_01_b(400)`, `interlaken_01_a(1680)`, `zurich_city_12_a(400)` are accurately represented. Although the boundaries in our results may lack the sharpness achieved by supervised baselines, our approach better preserves contour shapes, such as the front of the car in `interlaken_00_a(540)`, the arc of the tunnel in `interlaken_00_b(560)` and the pole in `zurich_city_13_a(260)`. This advantage is especially evident for thin objects like the sign pole in `interlaken_01_a(1680)` and `zurich_city_12_a(440)`, which are often challenging for supervised methods to capture accurately. Additionally, our self-supervised approach is immune to artifacts typically caused by the sporadic availability of ground truth at the image frame boundaries, resulting in smoother disparity maps free from discontinuity artifacts.

Several factors constrain the accuracy of our methods on these benchmarks, including the reliance on self-supervised learning with events only, a compact network architecture, the use of monocular depth estimation rather than stereo and the imperfect estimation of scaling factor for converting monocular depth to metric depth. While our aim is not to surpass state-of-the-art methods, we believe the quality of our depth predictions is sufficient to support downstream tasks like robot navigation.

4.2. Robotic Experiments

We first pretrain our network on the UZH-FPV dataset [9] using our self-supervised pipeline. This dataset was chosen for its diverse set of motion trajectories, enabling the network to learn a latent representation that generalizes well across various motion types. After pretraining, the network is deployed on a drone, where online learning (fine-tuning) is performed during flight. The network’s forward pass op-

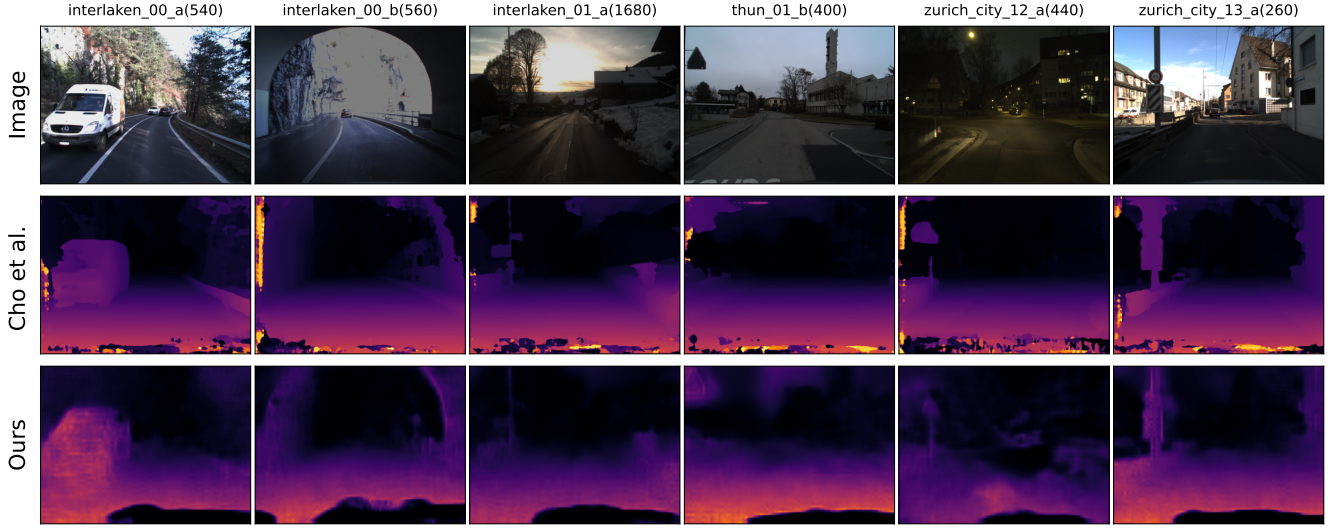


Figure 4. Qualitative results of disparity predictions on the DSEC disparity benchmark. Images are for visualization only, as disparity estimation is event-based. The same color map is applied to the disparity values from the stereo- and supervised-learning-based method from Cho et al. [8] and ours for easy comparison.

erates at an average speed of 30 Hz, with a backward pass and gradient update conducted every 10 forward passes. Following each gradient update, the state of the recurrent network is detached from the computational graph without resetting it. This approach ensures bounded memory usage, mitigates potential issues with gradient explosion or vanishing, and allows the network to retain temporal context effectively.

We show the metric improvements achieved during online learning in Fig. 7, where saved checkpoints are evaluated on a test sequence recorded in the same environment but with different placements for obstacles. The model shows significant improvement not only in the RSAT (ratio of squared average timestamps) metric, which is strongly correlated with the contrast maximization loss used to optimize the network, but also in MAE (mean absolute error) when compared against disparity ground truth. Additionally, the fine-tuning process is efficient, converging within just a few minutes of flight.

Qualitative results at different snapshots during online learning are presented in Fig. 6. Compared to step 0 (the pretrained model), the disparity values for certain close objects, such as the wall and poles, increase, as evidenced by the brightened colors in those regions. To highlight the advantages of pretraining, we also compare our model with a network initialized with random weights and trained using the same amount of online learning data, as shown in the last row of Fig. 6. The trained-from-scratch network fails to produce meaningful disparity maps within the flight’s limited timespan, underscoring the importance of pretraining for achieving fast and reliable adaptation during online

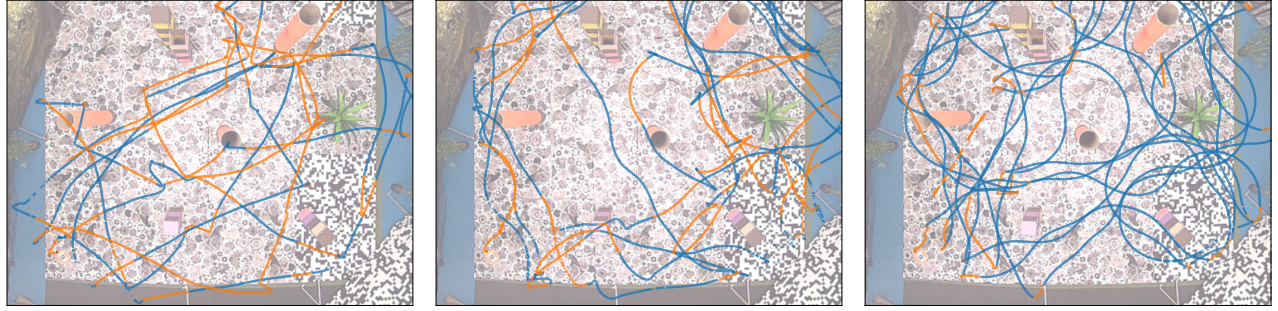
learning.

Finally, we plot the trajectories of the drone during the flight experiments under different settings in Fig. 5. During each experiment, the drone takes off and immediately starts to fly autonomously. A human pilot monitors the flight and intervenes if the drone is in a near collision with an obstacle. After the human pilot corrects for the collision course, the drone is switched to autonomous flying again. When the drone was initialized with random weights, the drone does not avoid obstacles and mostly fly with straight lines, as shown in Fig. 5a. This resulted in constant human interventions and a highest intervention rate of 50 %, determined by the ratio of time of human piloting during a flight.

When we start the experiment with a pre-trained network, the obstacle avoidance performance improves dramatically, lowering the intervention rate to 35 % in Fig. 5b. While the drone was already flying around obstacles, fine-tuning the model during flight further lowers the intervention rate to 11 %, as shown in Fig. 5c, allowing the drone to smoothly fly between obstacles with more curvy trajectories than in previous other settings.

5. Conclusion

We have improved the efficiency of self-supervised learning of monocular depth estimation from camera events, such that on-device learning of low-latency monocular depth and ego-motion becomes feasible. The proposed approach features more efficient splatting, and has been implemented in CUDA instead of PyTorch. For common event rates (e.g., 10e6 Ev/s), it uses 100× less memory and computational time. When trained and benchmarked on event cam-



(a) Initialize from a network with random weights. Intervention rate: 50%. (b) Initialize from pre-trained network, disable online learning. Intervention rate: 35%. (c) Initialize from pre-trained network, enable online learning. Intervention rate: 11%.

Figure 5. Top-view flight trajectories from various experiments. Blue trajectories represent autonomous flights, while orange trajectories indicate manual flights where human intervention was necessary to prevent potential collisions. The setup with online learning demonstrates the best obstacle avoidance performance, achieving the lowest intervention rate.

era datasets, our small recurrent network outperforms other self-supervised approaches on the MVSEC dataset and captures essential structures with sufficient quality to support downstream navigation tasks on the DSEC dataset. Furthermore, we demonstrate online learning on-board a small flying drone, and show the usability of the resulting depth for obstacle avoidance. Finally, we investigate various combinations of pre-training and on-board learning, showing that the latter leads to a flight intervention rate reduction from 35% to 11%.

Our work scratches at the surface of the unused potential of on-board, online self-supervised learning. The current results already demonstrate that online learning leads to better performance in the operational environment. This confirms that learning with samples from the test environment will be important for challenging vision tasks such as monocular depth estimation from events. Moreover, it is important to note that the performance gap between self-supervised learning and supervised learning is still substantial (see Tab. 2). This suggests that there is ample room for improvement of the self-supervised learning scheme, which may lead to a larger performance improvement after online refinement. Moreover, improved detail in the estimated depth maps will facilitate more complex obstacle avoidance and navigation behaviors. Future work under such conditions would be even better positioned to investigate the downstream behavioral advantages of online self-supervised depth learning.

Self-supervised learning has turned out to be instrumental for learning advanced AI methods on enormous, unlabelled datasets. The current work is a small step towards unlocking this type of learning’s second major advantage, i.e., strongly reducing the need for generalization by learning in the test environment. We expect this to form a key component of truly autonomous robots that can quickly and aptly adapt to their environment.

References

- [1] Anish Bhattacharya, Marco Cannici, Nishanth Rao, Yuezhan Tao, Vijay Kumar, Nikolai Matni, and Davide Scaramuzza. Monocular Event-Based Vision for Dodging Static Obstacles with a Quadrotor. In *8th Annual Conference on Robot Learning*, 2024. 3
- [2] Jiawang Bian, Zhichao Li, Naiyan Wang, Huangying Zhan, Chunhua Shen, Ming-Ming Cheng, and Ian Reid. Unsupervised Scale-consistent Depth and Ego-motion Learning from Monocular Video. In *Advances in Neural Information Processing Systems*. Curran Associates, Inc., 2019. 2, 3
- [3] Levi Burner, Anton Mitrokhin, Cornelia Fermüller, and Yiannis Aloimonos. EVIMO2: An Event Camera Dataset for Motion Segmentation, Optical Flow, Structure from Motion, and Visual Inertial Odometry in Indoor Scenes with Monocular or Stereo Algorithms. *arXiv:2205.03467 [cs]*, 2022. 1
- [4] Punarjay Chakravarty, Klaas Kelchtermans, Tom Roussel, Stijn Wellens, Tinne Tuytelaars, and Luc Van Eycken. CNN-based single image obstacle avoidance on a quadrotor. In *2017 IEEE International Conference on Robotics and Automation (ICRA)*, pages 6369–6374, 2017. 4
- [5] Kenneth Chaney, Fernando Cladera, Ziyun Wang, Anthony Bisulco, M. Ani Hsieh, Christopher Korpela, Vijay Kumar, Camillo J. Taylor, and Kostas Daniilidis. M3ED: Multi-Robot, Multi-Sensor, Multi-Environment Event Dataset. In *Proceedings of the IEEE/CVF Conference on Computer Vision and Pattern Recognition*, pages 4016–4023, 2023. 1
- [6] Yuhua Chen, Cordelia Schmid, and Cristian Sminchisescu. Self-Supervised Learning With Geometric Constraints in Monocular Video: Connecting Flow, Depth, and Camera. In *Proceedings of the IEEE/CVF International Conference on Computer Vision*, pages 7063–7072, 2019. 2
- [7] Hoonhee Cho and Kuk-Jin Yoon. Selection and cross similarity for event-image deep stereo. In *Computer Vision – ECCV 2022: 17th European Conference, Tel Aviv, Israel, October 23–27, 2022, Proceedings, Part XXXII*, page 470–486, Berlin, Heidelberg, 2022. Springer-Verlag. 5
- [8] Hoonhee Cho, Jae-Young Kang, and Kuk-Jin Yoon. Temporal event stereo via joint learning with stereoscopic flow.

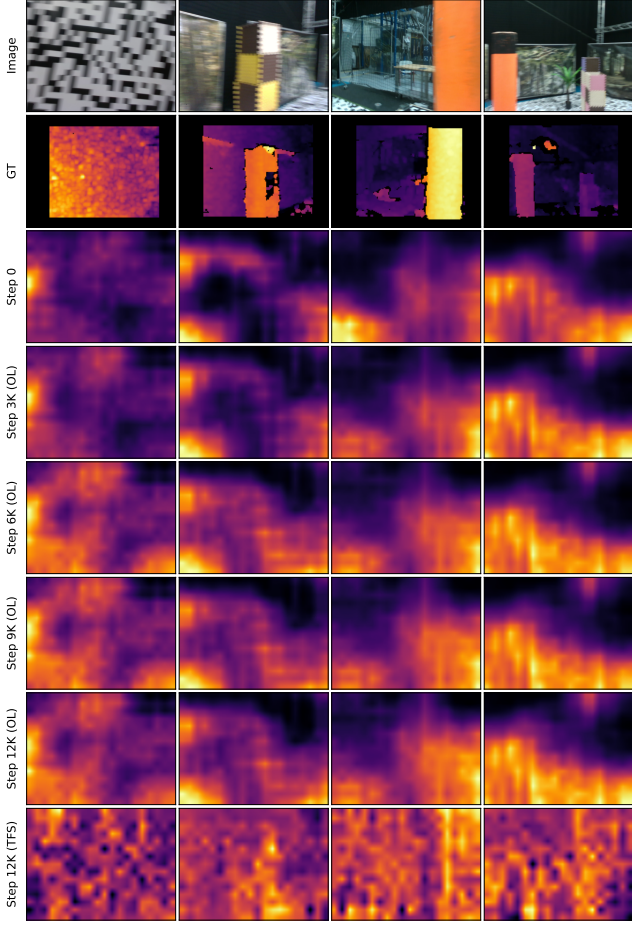


Figure 6. Qualitative visualization of disparity map evolution during online learning. Note that the image is for visualization purposes only, as disparity estimation is event-based. The same colour map is applied to predictions from all different models for easy comparison. The pre-trained network begins at step 0, followed by 12K steps of online learning (OL) with streaming event data during flight. For comparison, we also show the prediction quality of a randomly initialized network trained from scratch (TFS) for 12K steps.

- In *Computer Vision – ECCV 2024*, pages 294–314, Cham, 2025. Springer Nature Switzerland. 5, 6, 4
- [9] Jeffrey Delmerico, Titus Cieslewski, Henri Rebecq, Matthias Faessler, and Davide Scaramuzza. Are we ready for autonomous drone racing? the UZH-FPV drone racing dataset. In *IEEE Int. Conf. Robot. Autom. (ICRA)*, 2019. 4, 5
- [10] Zih-Sing Fu, Soumya Sudhakar, Sertac Karaman, and Vivienne Sze. DecTrain: Deciding When to Train a DNN Online, 2024. 2
- [11] Guillermo Gallego, Henri Rebecq, and Davide Scaramuzza. A Unifying Contrast Maximization Framework for Event Cameras, With Applications to Motion, Depth, and Optical Flow Estimation. In *Proceedings of the IEEE Conference on Computer Vision and Pattern Recognition*, pages 3867–3876, 2018. 1, 2, 3

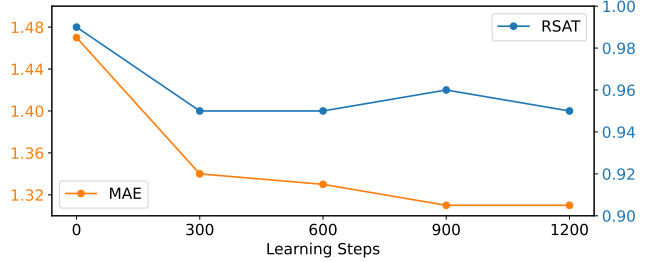


Figure 7. Mean absolute error (MAE) of disparity prediction and the ratio of squared average timestamp (RSAT) during online learning in flight. Model checkpoints were saved periodically and evaluated on a test sequence unseen by the model beforehand. 300 learning steps correspond to roughly 100 seconds of training during flight.

- [12] Guillermo Gallego, Mathias Gehrig, and Davide Scaramuzza. Focus Is All You Need: Loss Functions for Event-Based Vision. In *Proceedings of the IEEE/CVF Conference on Computer Vision and Pattern Recognition*, pages 12280–12289, 2019. 1, 2, 3
- [13] Guillermo Gallego, Tobi Delbrück, Garrick Orchard, Chiara Bartolozzi, Brian Taba, Andrea Censi, Stefan Leutenegger, Andrew Davison, Joerg Conradt, Kostas Daniilidis, and Davide Scaramuzza. Event-based Vision: A Survey. *IEEE Transactions on Pattern Analysis and Machine Intelligence*, pages 1–1, 2020. 1
- [14] Mathias Gehrig, Willem Aarents, Daniel Gehrig, and Davide Scaramuzza. Dsec: A stereo event camera dataset for driving scenarios. *IEEE Robotics and Automation Letters*, 2021. 1, 5
- [15] Stamatios Georgoulis, Weining Ren, Alfredo Bochicchio, Daniel Eckert, Yuanyou Li, and Abel Gawel. Out of the Room: Generalizing Event-Based Dynamic Motion Segmentation for Complex Scenes. In *2024 International Conference on 3D Vision (3DV)*, pages 442–452, 2024. 2
- [16] Clement Godard, Oisin Mac Aodha, Michael Firman, and Gabriel J. Brostow. Digging Into Self-Supervised Monocular Depth Estimation. In *Proceedings of the IEEE/CVF International Conference on Computer Vision*, pages 3828–3838, 2019. 2
- [17] Ariel Gordon, Hanhan Li, Rico Jonschkowski, and Anelia Angelova. Depth From Videos in the Wild: Unsupervised Monocular Depth Learning From Unknown Cameras. In *Proceedings of the IEEE/CVF International Conference on Computer Vision*, pages 8977–8986, 2019. 2, 3
- [18] Jesse Hagenars, Federico Paredes-Vallés, and Guido de Croon. Self-Supervised Learning of Event-Based Optical Flow with Spiking Neural Networks. In *Advances in Neural Information Processing Systems*, 2021. 2, 3
- [19] Friedhelm Hamann, Ziyun Wang, Ioannis Asmanis, Kenneth Chaney, Guillermo Gallego, and Kostas Daniilidis. Motion-prior Contrast Maximization for Dense Continuous-Time Motion Estimation, 2024. 2
- [20] Kevin Lamers, Sjoerd Tijmons, Christophe De Wagter, and Guido de Croon. Self-supervised monocular distance learn-

- ing on a lightweight micro air vehicle. In *2016 IEEE/RSJ International Conference on Intelligent Robots and Systems (IROS)*, pages 1779–1784, 2016. 3
- [21] Hanhan Li, Ariel Gordon, Hang Zhao, Vincent Casser, and Anelia Angelova. Unsupervised Monocular Depth Learning in Dynamic Scenes. In *Proceedings of the 2020 Conference on Robot Learning*, pages 1908–1917. PMLR, 2021. 2
- [22] Cheng Liu, Yingfu Xu, Erik-Jan van Kampen, and Guido de Croon. Nano Quadcopter Obstacle Avoidance with a Lightweight Monocular Depth Network. *IFAC-PapersOnLine*, 56:9312–9317, 2023. 3, 4
- [23] Steven Macenski, Tully Foote, Brian Gerkey, Chris Lalancette, and William Woodall. Robot operating system 2: Design, architecture, and uses in the wild. *Science robotics*, 7(66):eabm6074, 2022. 4
- [24] Federico Paredes-Vallés, Kirk Y. W. Schepers, Christophe De Wagter, and Guido C. H. E. de Croon. Taming Contrast Maximization for Learning Sequential, Low-latency, Event-based Optical Flow. In *Proceedings of the IEEE/CVF International Conference on Computer Vision*, pages 9695–9705, 2023. 1, 2, 3, 4
- [25] F. Paredes-Vallés, J. J. Hagenaars, J. Dupeyroux, S. Stroobants, Y. Xu, and G. C. H. E. de Croon. Fully neuromorphic vision and control for autonomous drone flight. *Science Robotics*, 9:eadi0591, 2024. 1
- [26] Anurag Ranjan, Varun Jampani, Lukas Balles, Kihwan Kim, Deqing Sun, Jonas Wulff, and Michael J. Black. Competitive Collaboration: Joint Unsupervised Learning of Depth, Camera Motion, Optical Flow and Motion Segmentation. In *Proceedings of the IEEE/CVF Conference on Computer Vision and Pattern Recognition*, pages 12240–12249, 2019. 2
- [27] Shintaro Shiba, Yannick Klose, Yoshimitsu Aoki, and Guillermo Gallego. Secrets of Event-based Optical Flow, Depth and Ego-motion Estimation by Contrast Maximization. *IEEE Transactions on Pattern Analysis and Machine Intelligence*, pages 1–18, 2024. 1, 2
- [28] Yihong Sun and Bharath Hariharan. Dynamo-Depth: Fixing Unsupervised Depth Estimation for Dynamical Scenes. In *Thirty-Seventh Conference on Neural Information Processing Systems*, 2023. 2
- [29] Kevin van Hecke, Guido de Croon, Laurens van der Maaten, Daniel Hennes, and Dario Izzo. Persistent self-supervised learning: From stereo to monocular vision for obstacle avoidance. *International Journal of Micro Air Vehicles*, 10(2):186–206, 2018. 2
- [30] Sudheendra Vijayanarasimhan, Susanna Ricco, Cordelia Schmid, Rahul Sukthankar, and Katerina Fragkiadaki. SfM-Net: Learning of Structure and Motion from Video, 2017. 2
- [31] Niclas Vödisch, Kürsat Petek, Wolfram Burgard, and Abhinav Valada. CoDEPS: Online Continual Learning for Depth Estimation and Panoptic Segmentation. In *Robotics: Science and Systems XIX*, 2023. 2
- [32] Chaoyang Wang, José Miguel Buenaposada, Rui Zhu, and Simon Lucey. Learning Depth From Monocular Videos Using Direct Methods. In *Proceedings of the IEEE Conference on Computer Vision and Pattern Recognition*, pages 2022–2030, 2018. 3
- [33] Rui Wang, Stephen M. Pizer, and Jan-Michael Frahm. Recurrent Neural Network for (Un-)Supervised Learning of Monocular Video Visual Odometry and Depth. In *Proceedings of the IEEE/CVF Conference on Computer Vision and Pattern Recognition*, pages 5555–5564, 2019. 2
- [34] C. Ye, A. Mitrokhin, C. Fermüller, J. A. Yorke, and Y. Aloimonos. Unsupervised Learning of Dense Optical Flow, Depth and Egomotion with Event-Based Sensors. In *2020 IEEE/RSJ International Conference on Intelligent Robots and Systems (IROS)*, pages 5831–5838, 2020. 2
- [35] Zhichao Yin and Jianping Shi. GeoNet: Unsupervised Learning of Dense Depth, Optical Flow and Camera Pose. In *Proceedings of the IEEE Conference on Computer Vision and Pattern Recognition*, pages 1983–1992, 2018. 2
- [36] Tinghui Zhou, Matthew Brown, Noah Snavely, and David G. Lowe. Unsupervised Learning of Depth and Ego-Motion from Video. In *2017 IEEE Conference on Computer Vision and Pattern Recognition (CVPR)*, pages 6612–6619, 2017. 2, 3
- [37] Alex Zihao Zhu, Dinesh Thakur, Tolga Özaslan, Bernd Pfommer, Vijay Kumar, and Kostas Daniilidis. The Multivehicle Stereo Event Camera Dataset: An Event Camera Dataset for 3D Perception. *IEEE Robotics and Automation Letters*, 3:2032–2039, 2018. 1, 4
- [38] Alex Zihao Zhu, Liangzhe Yuan, Kenneth Chaney, and Kostas Daniilidis. Unsupervised Event-Based Learning of Optical Flow, Depth, and Egomotion. In *Proceedings of the IEEE/CVF Conference on Computer Vision and Pattern Recognition*, pages 989–997, 2019. 1, 2, 5
- [39] Junyu Zhu, Lina Liu, Bofeng Jiang, Feng Wen, Hongbo Zhang, Wanlong Li, and Yong Liu. Self-Supervised Event-Based Monocular Depth Estimation Using Cross-Modal Consistency. In *2023 IEEE/RSJ International Conference on Intelligent Robots and Systems (IROS)*, pages 7704–7710, 2023. 2, 5

On-Device Self-Supervised Learning of Low-Latency Monocular Depth from Only Events

Supplementary Material

6. Optimized warping and splatting

Fig. 8 visualizes, on a high level, how our optimizations with respect to warping sets of events to different reference times are reducing runtime and memory consumption by preventing unnecessary warping operations.

7. Extra DSEC qualitative results

We present additional qualitative results from the DSEC test set in Fig. 9. While the self-supervised results exhibit less sharp boundaries, they are free from many artifacts commonly introduced by supervised learning, such as discontinuities at frame boundaries and difficulties in handling thin objects.

8. More robot experiment results

Figs. 10 to 13 show extended qualitative results for four unseen scenes during a flight experiment. Looking at Fig. 10, we see that network’s ability to maximize the contrast of the image of warped events increases quickly from ‘step 0’ (only pre-training) to ‘step 3k’ (pre-training + 100 seconds of learning). While this improvement in terms of contrast maximization loss may be mostly due to just learning to increase the magnitude of the optical flow (as shown by the change from orange to purple in column 3, and black to red in column 5) through scaling depth and ego-motion, subsequent learning steps improve the depth map in more sophisticated ways, judging from the disappearance of the wrong ‘depth gap’ in the center of the disparity images in the third and fourth column. Similar priorities in learning (first scaling, then the rest) can be seen in the other scenes.

9. Training details

For offline training on datasets, we train for 50 epochs with the Adam optimizer and a learning rate of 1e-4. For contrast maximization, we accumulate 10 bins of events, and warp all events to all bin edges. Furthermore, we set the weight for the geometric consistency loss $\lambda = 0.05$. For on-device learning, we lower the learning rate to 1e-5. Other specifics vary per dataset, and are mentioned below. In all cases, event streams are rectified.

For MVSEC, we train on `outdoor_day2` with input bins of 20 ms of events. We use a batch size of 8, and augment the data with polarity and left-right flips. Training takes around 50 minutes on an RTX 4090.

For DSEC, we train on the daylight sequences

in the training set (`interlaken_00_*` and `zurich_city_{04,05,06,07,08,11}_*`). We leave `thun_00_a` for validation. Because of DSEC’s high event density and large frames, we lower the batch size to 4, and bin events to 10 ms frames with a cap of 100k events per bin (if there are more events, we end the bin prematurely; we do not discard events). In addition to polarity and left-right flips, we augment by reversing the time dimension, as we saw that this lessened border artifacts with wrong optical flows. Training takes around 11 hours on an RTX 4090.

For UZH-FPV, we train on the forward indoor sequences (`indoor_forward_{3,5,6,7,9}_davis_with_gt` and `indoor_forward_{8,11,12}_davis`). Sequence `indoor_forward_10_davis_with_gt` is left for validation. We use 10 ms bins of events, a batch size of 8 and polarity and left-right flips. Training takes approximately 30 minutes on an RTX 4090.

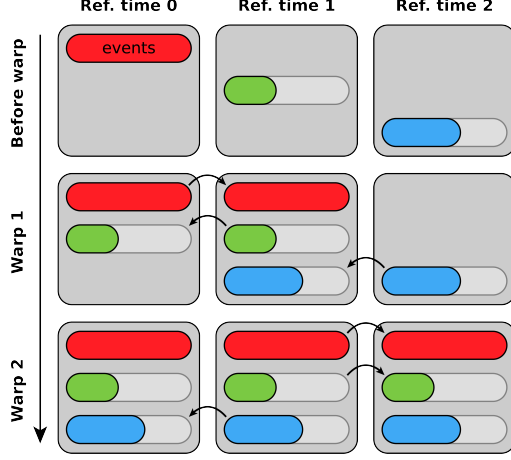
10. Network details

We make use of a small convolutional recurrent network to predict depth and ego-motion. The encoder and memory backbone are shared between the depth and ego-motion decoders. Tab. 3 lists the details per layer. In addition, we make use of ELU activations as we experienced dying ReLUs. Also, to prevent border artifacts, we use reflect padding for all convolutional layers.

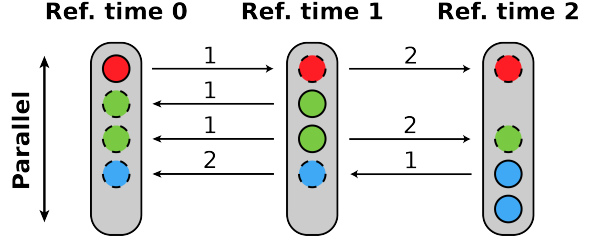
11. Robot details

We built a 5-inch quadrotor for our robotic experiments. The drone is equipped with on-board sensors that provide the flight controller with all relevant information to follow high-level control commands. More specifically, the EKF running on the Kakute H7 Mini flight controller fuses IMU measurements with velocity and height measurements coming from a MTF-01 optical flow/range sensor into a stable position and velocity estimate. This allows a neural network (like our depth network) to give high-level commands like velocity setpoints or rotational rates.

All relevant components on the drone, along with their weight and power consumption, can be found in Tab. 4. All separate modules on the Jetson Orin NX are connected via ROS2, which also allows for logging to rosbags. ROS2 can also be connected via UART to the internal publish-subscribe messaging API that is used in the PX4 flight controller firmware.



(a) Warping events to multiple reference times in a batched manner involves zero-padding all bins to the same length (light-gray extensions), leading to unnecessary warping operations. Furthermore, events that were already warped out of the image space (and can be discarded) will still be warped.



(b) Warping all events individually in parallel does away with padding and allows to warp only those events that are still in the image space, giving the minimal amount of warping operations necessary.

Figure 8. Comparison of warping three bins of events to three reference times. Events originating from different bins have different colors. At every stage of warping (1, 2), events get warped to a neighboring bin, until we have reached all three reference times.

Table 3. Network layer details. Unless specified otherwise, we use ELU activations, and a kernel size of 3, biases and ‘reflect’ padding for convolutional layers. Total parameter count is 430,416.

	Layer type	Input shape	Output shape	# Parameters
Encoder	Conv2D (ksize=7, stride=2)	(2, H , W)	(16, $H/2$, $W/2$)	1,584
	ResidualConv2D (stride=2)	(16, $H/2$, $W/2$)	(32, $H/4$, $W/4$)	18,528
	ResidualConv2D (stride=2)	(32, $H/4$, $W/4$)	(64, $H/8$, $W/8$)	73,920
Memory	ConvGRU	(64 + 64, $H/8$, $W/8$)	(64, $H/8$, $W/8$)	221,568
Depth	Conv2D	(64, $H/8$, $W/8$)	(64, $H/8$, $W/8$)	36,928
	Conv2D (bias=False) w/ SoftPlus	(64, $H/8$, $W/8$)	(1, $H/8$, $W/8$)	576
	Upsample (scale=8, ‘bilinear’)	(1, $H/8$, $W/8$)	(1, H , W)	
Ego-motion	Conv2D (stride=2)	(64, $H/8$, $W/8$)	(64, $H/16$, $W/16$)	36,928
	Conv2D (stride=2)	(64, $H/16$, $W/16$)	(64, $H/32$, $W/32$)	36,928
	Conv2D (bias=False) w/ Identity	(64, $H/32$, $W/32$)	(6, $H/32$, $W/32$)	3,456
	AdaptiveAvgPool2D	(6, $H/32$, $W/32$)	(6, 1, 1)	

The power consumption during flight is measured by keeping track of the total mAh consumed by over two flight tests. Together with the measured power consumption of the Jetson using `jtop` and the expected maximum power draw of both cameras, this allows us to calculate the power consumption of the drone (see Tab. 4).

Table 4. List of hardware components used during robotic experiments. Power consumption estimates are obtained from Jetson’s `jtop`^{*}, battery drain during flight experiments[†], or component datasheets[‡].

Component	Product	Mass [g]	~Power [W]
Frame	Armattan Marmotte 5 inch		
Motors	Emax Eco II Series 2306		
Propellers	Ethix S5 5 inch	455	200 [†]
Flight controller	Holybro Kakute H7 Mini		
Optical flow & range sensor	MicoAir MTF-01		
ESC	Holybro Tekko32 F4 4in1 mini 50A BL32		
Battery	iFlight Fullsend 4S 3000mAh Li-Ion	208	-
On-board compute	NVIDIA Jetson Orin NX 16GB & DAMIAO v1.1 carrier board	62	9 [*]
Event camera	iniVation DVXplorer Micro	22	max 0.7 [‡]
Stereo camera	Intel RealSense D435i	75	max 3.5 [‡]
Total	-	822	213.2

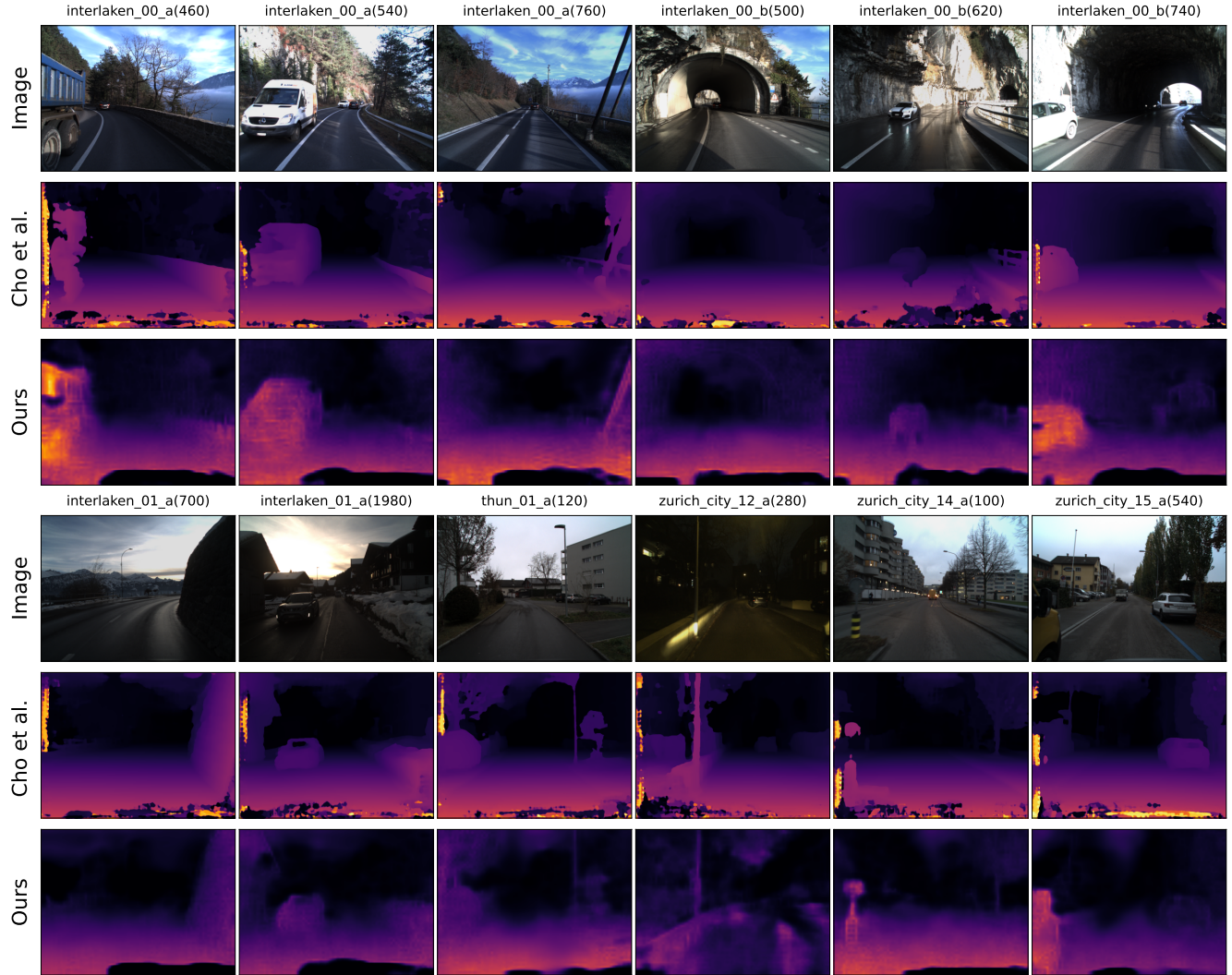


Figure 9. Additional qualitative results of disparity predictions on the DSEC disparity benchmark. Images are for visualization only, as disparity estimation is event-based. The same color map is applied to the disparity values from the stereo- and supervised-learning-based method from Cho et al. [8] and ours for easy comparison.

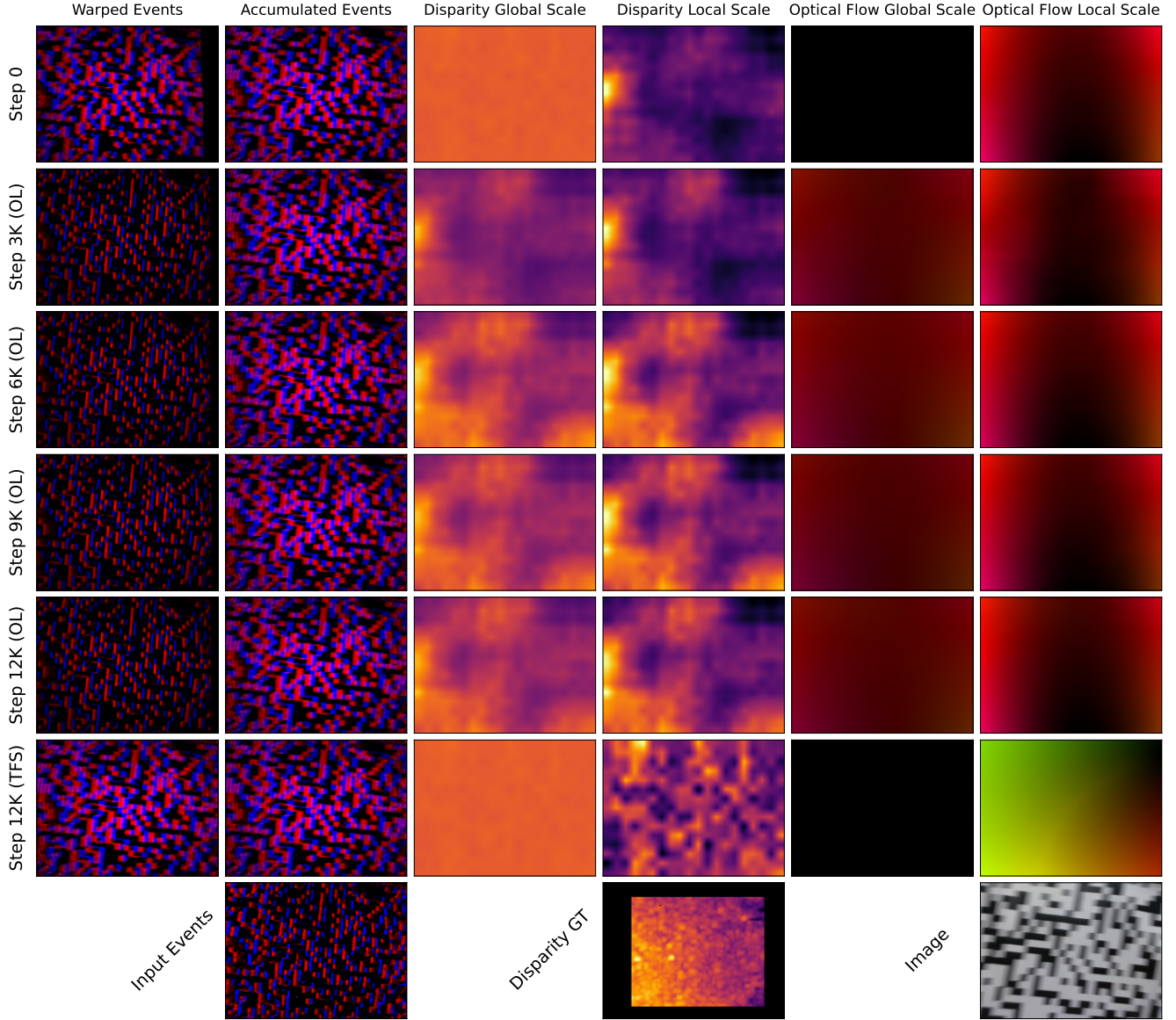


Figure 10. Extended qualitative results on unseen data from a flight test recording. From top to bottom, we evaluate a pre-trained-only network ('step 0'), then four networks after increasing amounts of online learning (OL), and finally a network trained-from-scratch. The bottom row starts with the single 20 ms bin of events currently seen by the network. The rest of the second column shows the accumulated events (multiple bins) in the current contrast maximization loss window. Applying the iterative warp by the optical flow constructed from depth and ego-motion gives the warped and deblurred events in the first column. Columns three and four show disparity at a global (colormap shared between rows) and local (colormap for only that row) scale. The last two columns show optical flow constructed from depth and ego-motion with global and local colormaps, respectively.

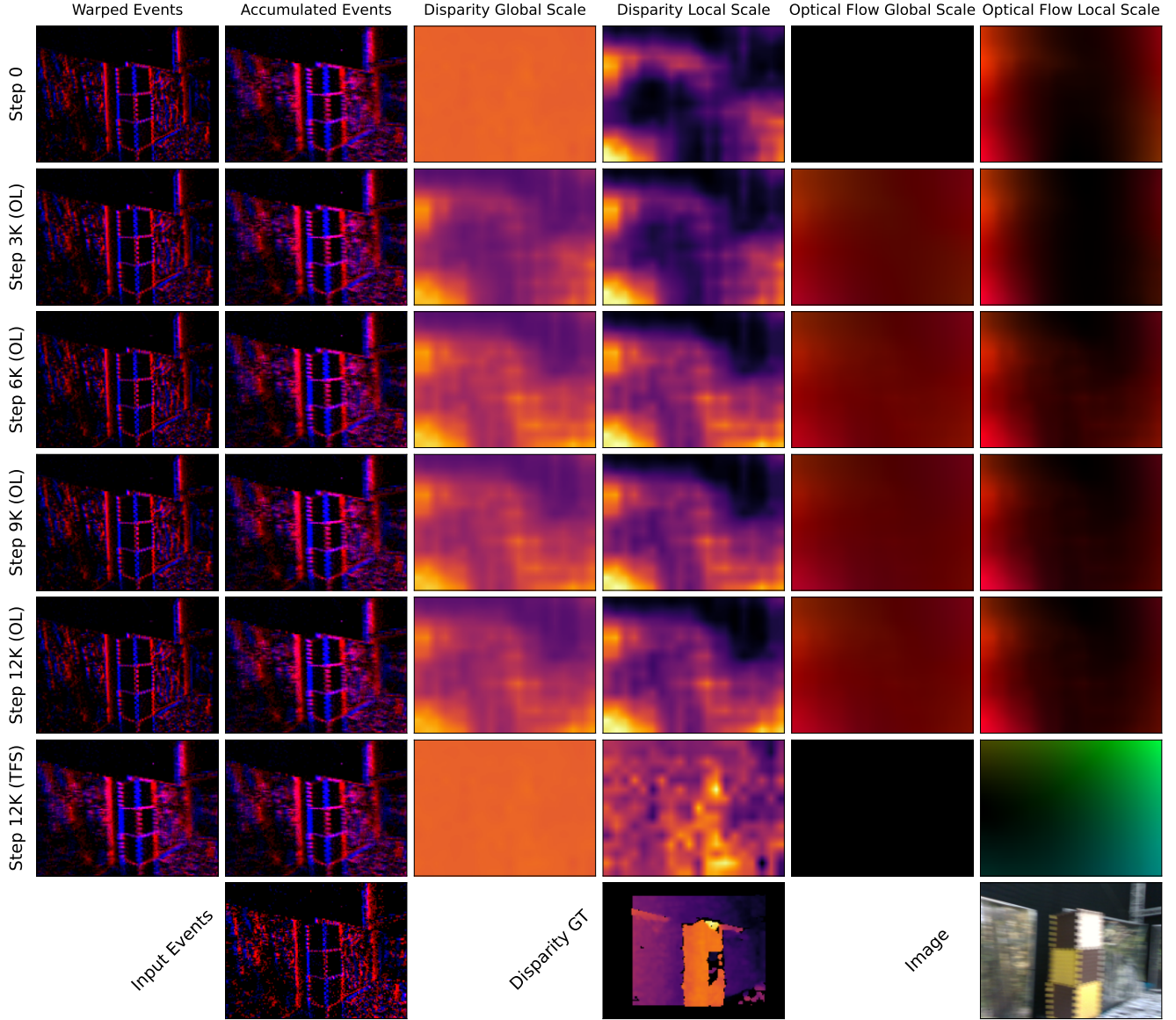


Figure 11. Extended qualitative results on unseen data from a flight test recording. From top to bottom, we evaluate a pre-trained-only network ('step 0'), then four networks after increasing amounts of online learning (OL), and finally a network trained-from-scratch. The bottom row starts with the single 20 ms bin of events currently seen by the network. The rest of the second column shows the accumulated events (multiple bins) in the current contrast maximization loss window. Applying the iterative warp by the optical flow constructed from depth and ego-motion gives the warped and deblurred events in the first column. Columns three and four show disparity at a global (colormap shared between rows) and local (colormap for only that row) scale. The last two columns show optical flow constructed from depth and ego-motion with global and local colormaps, respectively.

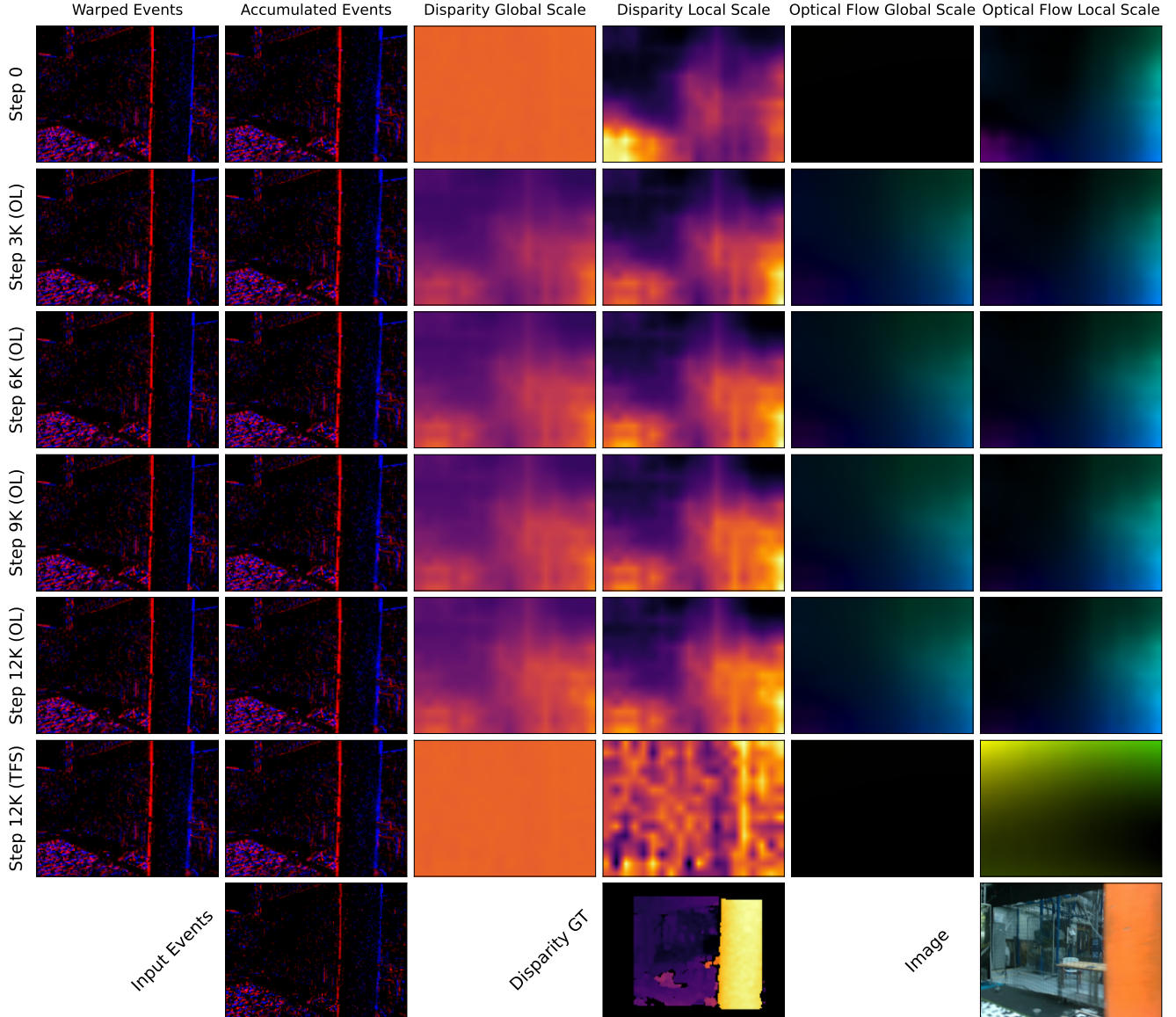


Figure 12. Extended qualitative results on unseen data from a flight test recording. From top to bottom, we evaluate a pre-trained-only network ('step 0'), then four networks after increasing amounts of online learning (OL), and finally a network trained-from-scratch. The bottom row starts with the single 20 ms bin of events currently seen by the network. The rest of the second column shows the accumulated events (multiple bins) in the current contrast maximization loss window. Applying the iterative warp by the optical flow constructed from depth and ego-motion gives the warped and deblurred events in the first column. Columns three and four show disparity at a global (colormap shared between rows) and local (colormap for only that row) scale. The last two columns show optical flow constructed from depth and ego-motion with global and local colormaps, respectively.

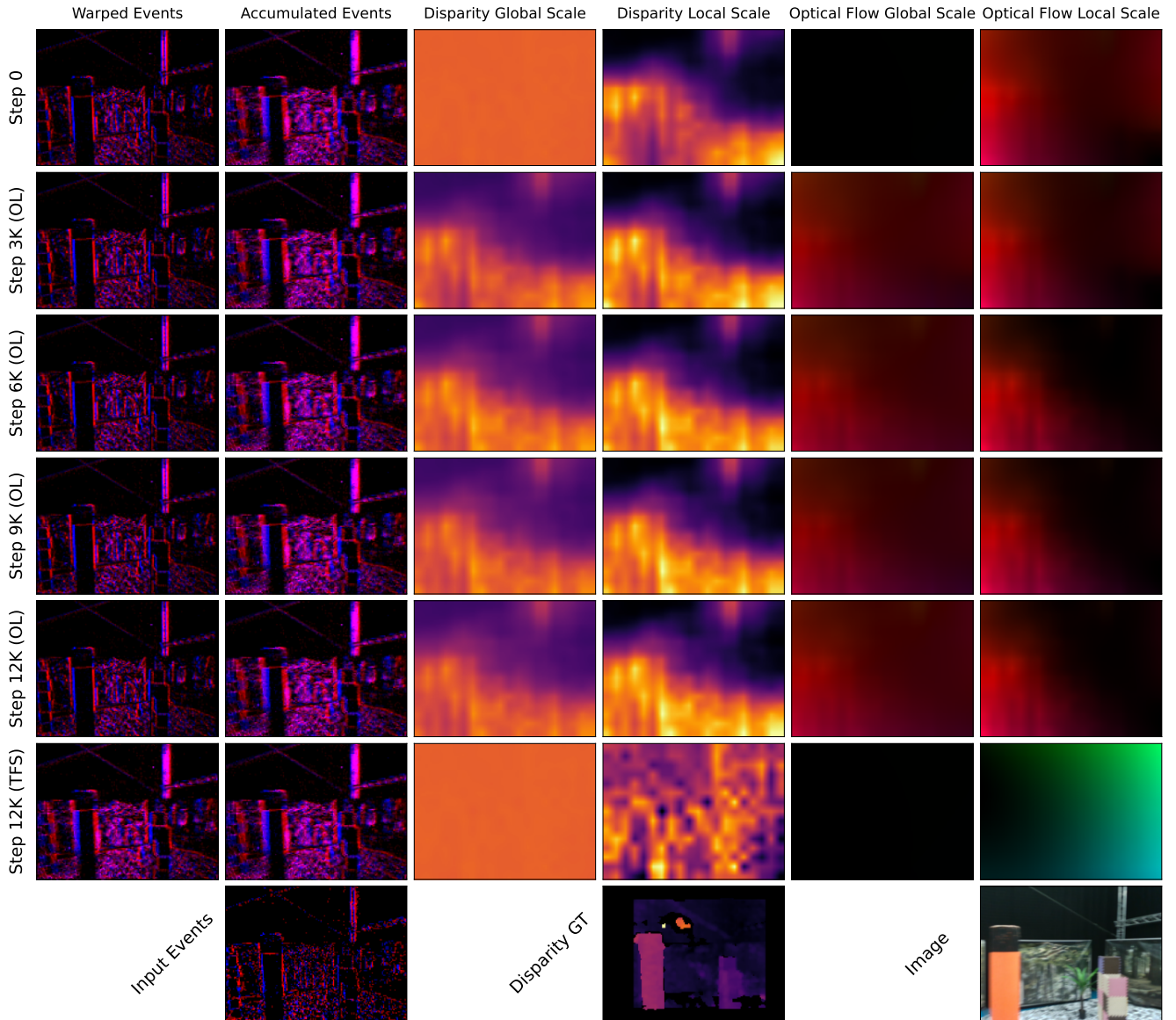


Figure 13. Extended qualitative results on unseen data from a flight test recording. From top to bottom, we evaluate a pre-trained-only network ('step 0'), then four networks after increasing amounts of online learning (OL), and finally a network trained-from-scratch. The bottom row starts with the single 20 ms bin of events currently seen by the network. The rest of the second column shows the accumulated events (multiple bins) in the current contrast maximization loss window. Applying the iterative warp by the optical flow constructed from depth and ego-motion gives the warped and deblurred events in the first column. Columns three and four show disparity at a global (colormap shared between rows) and local (colormap for only that row) scale. The last two columns show optical flow constructed from depth and ego-motion with global and local colormaps, respectively.